A1
Deformation of the Taconic Sequence, western Vermont and eastern New York

Art Goldstein, Department of Geology, Colgate University, Hamilton, New York 13346
Yu-Chang Chan, Department of Geology and Geophysics, University of Connecticut, Storrs, Connecticut 06269
Jim Pickens, Department of Geological Sciences, University of Massachusetts, Amherst, Massachusetts 01003
Jean Crespi, Department of Geology and Geophysics, University of Connecticut, Storrs, Connecticut 06269

INTRODUCTION

The Taconics are a series of thrust sheets which lie along the western edge of the northern Appalachians in western Vermont, Massachusetts and Connecticut and eastern New York (figure 1). The thrust sheets contain metamorphosed Cambro-Ordovician argillaceous rocks with minor arenites and limestones. Along the western edge of the Taconics in the lowest thrust sheet, the metamorphic grade is low and the rocks contain a prominent slaty cleavage. To the east and in higher thrust sheets the slaty cleavage is overprinted by crenulation cleavages, the metamorphic grade is higher and phyllites and schists are common. The Taconic thrust sheets sit on autochthonous to para-autochthonous Cambro-Ordovician carbonates or middle Ordovician flysch. The geology of the Taconics has been used as a model of relating plate tectonics to the evolution of mountain belts (Bird and Dewey, 1970; Rowley and Kidd, 1981). Despite some differences, most workers agree on the basic plate tectonic setting of the Taconic orogeny (e.g. Rowley and Kidd, 1981, Stanley and Ratcliffe , 1988). Rocks contained within the Taconic klippe were deposited on the slope and rise of the early Paleozoic passive margin of North America from Cambrian through middle Ordovician time. In the middle Ordovician, the North America passive margin reached the west-facing Taconic subduction zone and collision produced the deformation now seen within the thrust sheets as well as creating the thrust sheets themselves. This trip will examine the details of Taconic deformation within the notrthern part of the thrust sheets (figure 1) and, thus, can be viewed as an investigation of deformation associated with arc-continent collision.

Taconic Stratigraphy. The stratigraphy of the Taconics was originally established by Zen (1961) and was later redefined by Rowley et al. (1979). As subdivided by Rowley et al. (1979), the general stratigraphy within the northern Taconics consists of six formations. The lowest formation, the Bomoseen, is largely clastic with overlying formations generally composed of slates and silty-slates. Limestones and sandstones are locally present, but volumetrically insignificant. The slatey formations are distinguished principally by color. A regional angular unconformity occurs at the top of the Taconic stratigraphy with a shale-greywacke

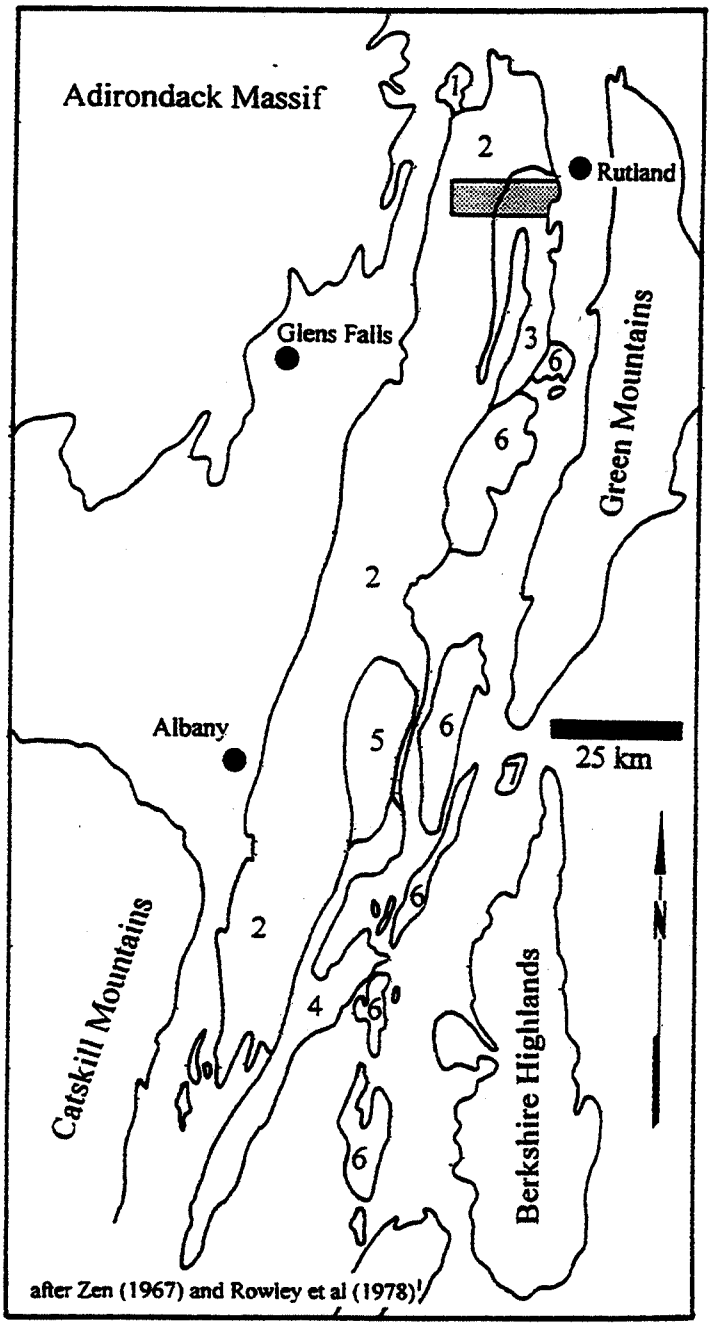

Figure 1. Map showing locations of the major geological features of eastern New York and western Vermont and Massachusetts. Taconic thrust sheets are indicated by numbers; 1-Sunset Lake slice; 2-Giddings Brook slice; 3-Bird Mountain slice; 4-Chathan slice; 5-Rensselaer Plateau slice; 6-Dorsett Mountain slice; 7- Greylock slice.

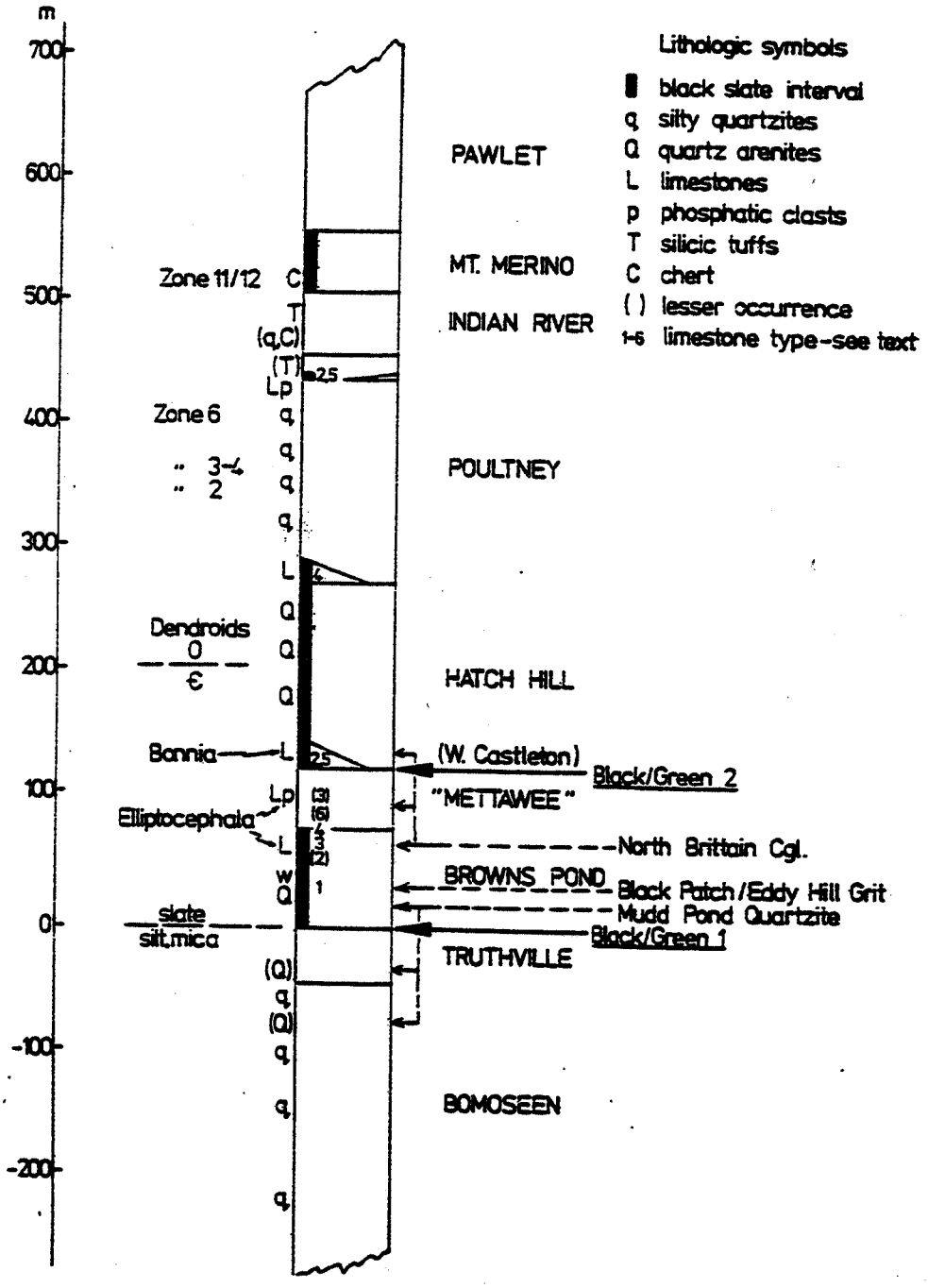

Figure 2. Stratigraphy of the Giddings Brook slice, from Rowley et al, 1979

unit (Pawlet fm) overlying it. The formations are laterally continuous and have been used successfully for mapping over large distances.

General Structural Geology. The most prominent structures of the Taconic klippe and folds and thrust faults (figure 3). The most prominent thrust faults bound the different klippe and minor thrusts within klippe are locally present. In the region of this field trip, and for most of length of the Taconics, the lowest thrust slice is the Giddings Brook slice (figure 1) bounded on bottom by the Giddings Brook fault and above by the Bird Mountain fault. In the northern Taconics, the next highest slice is the Bird Mountain slice. Both the Bird Mountain and Giddings Brook faults truncate isoclinal folds which dominate the structures within thrust sheets (figure 3). The largest folds have wavelengths of 1 - 1.5 km and amplitudes of 1.5 - 3 km. Fold axes trend roughly N-S and plunge shallowly to the north and south (figure 4). Axial planes strike roughly N-S and dip eastward at angles from 20-60°. The hinges are very tight and are only rarely exposed. The folds have a prominent axial plane slaty cleavage which makes the rocks commercially usable. Because the folds are isoclinal and have an axial plane cleavage, bedding and cleavage are parallel on limbs and transect each other at or close to fold hinges.

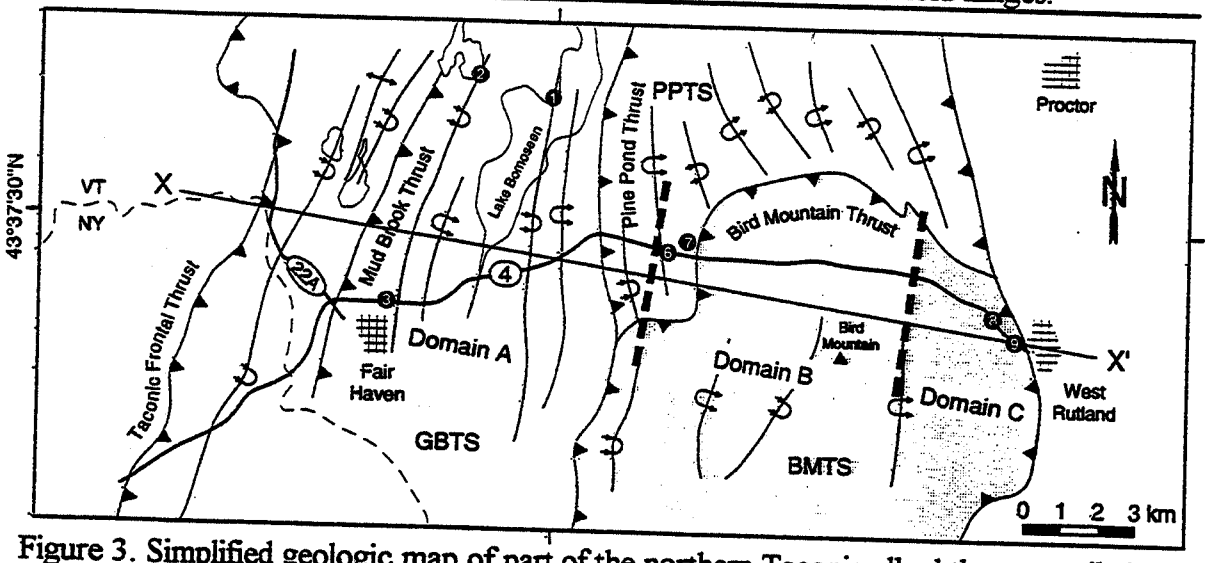

Figure 3. Simplified geologic map of part of the northern Taconic allochthon compiled from Zen (1961) and Fisher et al. (1970). Some stop locations are shown by numbered black circles.

Timing of Deformations. A reasonably precise relative timing of various structural elements can be constructed from basic field relations and cross-cutting relationships. The earliest structures recognized are early thrust faults (folded by isoclinal folds) and an early cleavage (S_1). Early thrusts are rare and evidence for the S_1 cleavage is seen almost exclusively in thin section. The origin of S_1 is a matter of speculation. We are confident, however, that its origins are tectonic rather than compactional as it commonly is not parallel to bedding. Folds are the next youngest structures. Locally, early thrust faults

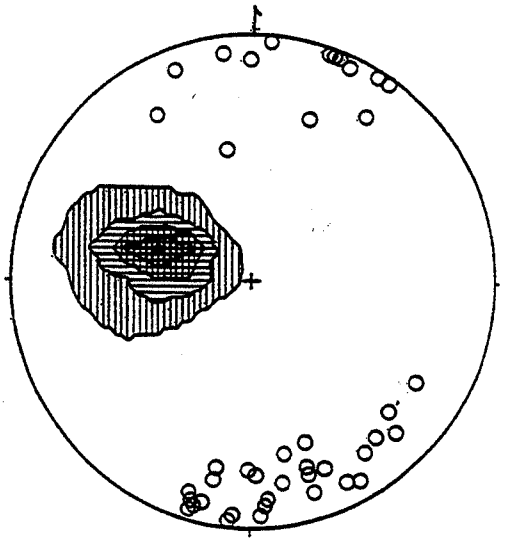

Figure 4. Lower hemisphere, equal-area projection of 600 poles to slaty cleavage (S_2, contours) and 42 measured fold axes and bedding-cleavage intersections (open circles). Contours are 1, 5, 10, 15 and 20% per 1% area

are folded, revealing the timing between the early faults and the folds, but any possible relationship between fold formation and the S_1 cleavage has yet to be determined. Thrust faulting continued after folding as is evidenced by both the Bird Mountain and Giddings Brook faults truncation of folds. The Bird Mountain fault, however, is older than the Giddings Brook fault based on relationships between the faults and the main slaty cleavage (S_2). The Bird Mountain fault is cut by S_2 and, thus, must pre-date it. The imposition of this cleavage on previously formed folds is most likely responsible for tightening the folds to their isoclinal geometry. The finite strain associated with cleavage formation is discussed below. Unlike the Bird Mountain fault, the Giddings Brook fault cuts the S_2 cleavage and last motion along it is the youngest event evidenced in the northern Taconics. Locally within the Giddings Brook slice and pervasively in its eastern portion and within the Bird Mountain slice late crenulation cleavages are present. Two principal sets occur with the youngest being present only in the easternmost part of the northern Taconics. The interpretation of these cleavage is discussed below.

For the most part, veins are uncommon in the northern Taconics but are present within the northern Taconics and will be visited by this trip. Three different vein families are present, although the timing of vein formation and its significance is a matter of continuing study. Some veins are clearly early as they are found folded and boudinaged. Other veins form in en-echelon sigmoidal arrays and may represent more than one period of veining. Some of these veins may be syn-folding whereas others are clearly post-folding. Some of these veins arrays are indicative of dip-slip ductile shearing whereas others indicate strike-slip deformation. Finally, one can find meter-scale bull quartz veins which cut all other structures and fabrics and are the latest veins to have formed in the northern Taconics.

FINITE AND INCREMENTAL STRAIN
(Goldstein and Pickens)

Considerable effort has been expended in analysis of both finite and incremental strain, especially in the Giddings Brook slice, which contains many strain indicators. Finite strain has been investigated using reduction spots (Goldstein et al, 1995a; Hoak, 1992 and Wood, 1974) and recently by measuring deformed graptolites (Goldstein et al, in press). This trip will visit localities used for both studies. In addition, incremental strains have been investigated using pyrite framboid pressure shadows (Cushing and Goldstein, 1990; Chan and Crespi, 1995) and pyrite porphyroblast pressure shadows (Pickens, 1993). Whereas the finite strain results are quite consistent, there are considerable differences in both the form and interpretation of pressure shadows observed by different workers, suggesting that none of us has fully determined what the complete incremental strain history is for these rocks. The implications of incremental strains are most significant with respect to the origin of the main slaty cleavage (S_2) and one view is expressed below. This topic is one which is still being debated by the authors.

Finite strain results. Pale green spots in the Mettawee fm. allow the measurement of finite strain at a number of localities (Goldstein et al, 1995a; Hoak, 1992; Wood, 1974). Spots occur in two general forms; nearly perfect ellipsoids and irregular blotches. The ellipsoids lie with their XY planes parallel to the plane of the main slaty cleavage (S_2) and must have begun as nearly perfect spheres or ellipsoids. Goldstein et al. (1995a) measured reduction spots are 7 localities in the Giddings Brook slice and another three sites were measured by Hoak (1992) and Wood (1974). All results agree well, lying in the field of apparent flattening on a flinn diagram and are arrayed along a horizontal trend (Fig 5). This pattern indicates that the difference in strain state between sites with lower strain and sites with higher strain lies in the ratio between Y and Z whereas the ratio between X and Y remains largely unchanged. Because reduction spots yield only strain ratios rather than absolute strains, there is an inherent ambiguity in their interpretation. This is especially true when it comes to determining volume changes which may have accompanied slaty cleavage development. One may interpret the variation in strain as reflective of constant volume deformation or as indicating considerable loss of volume. We do not favor the constant volume interpretation as it requires considerable elongation in Y to maintain a nearly constant XY ratio. None of the incremental strain work has yielded any indication of elongation in Y. Thus, our favored interpretation is that the shortening in Z was accommodated by loss of material through dissolution. Our calculations (Goldstein et al, 1995a) suggest that an average of 55% of the original solid volume of rock was lost at the most highly strained site. This number is a minimum because of assumptions which had to be made before the calculation could be done.

Reduction spots are inherently ambiguous, as noted above, because they yield strain rations rather than absolute strains. Absolute strains can be measured, however, through study of deformed graptolites (Goldstein et al, in press). Graptolites were

colonial planktonic organisms which were abundant during lower Paleozoic time. For

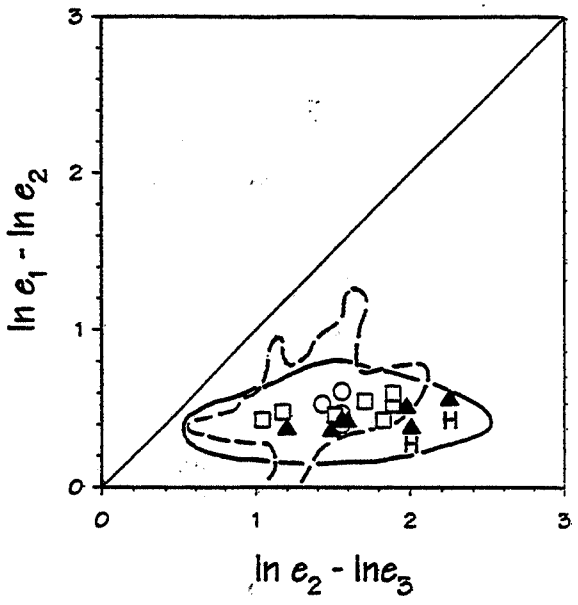

Figure 5. Summary of reduction spot strain measurements from the northern Giddings Brook slice. Black triangles are site averages measured by Goldstein et al. (1995a); open squares are from Wood (1974) and open circles are from Hoak (1992). The solid line shows the range of data measured by Hoak (1992) and the dashed line shows the range of values from slates in the Taconics and Wales measured by Wood (1974).

some species, certain dimensions were constant so that, in the deformed state, one can determine strain by measuring those dimensions and using the formula:

$$e=l_f-l_o/l_o$$

in which l_f represents the final length of a line (dimension in deformed state) and l_o represents the original length of a line (dimension in the undeformed state). For graptolites, the spacing between thecae is used (figure 6). By measuring enough graptolites which lie at different angles to principal strains one can define the two dimensional strain for the bedding plane, the plane which contains the graptolites. By measuring graptolites on the limbs of folds, in which bedding and cleavage are parallel, one derives the X and Y components of strain and measuring at hinges of folds, in which bedding and cleavage are perpendicular, one derives the Z component of strain. We have done this for five sites at limbs of folds and two at hinges, with another two sites lying between limb and hinge. e_1 (X) ranges from 110% to 30% with an average of 55%, e_2 (Y) ranges from 0% to -40% with an average of -22% and e_3 (Z) ranges from -60% to -80% with an average of -70%. Thus, we find that the absolute finite strain in these slates is constrictional (one elongation and two shortenings). The principal strains can be used to determine volume changes from the following relationship:

$$\ln (1+\Delta) = \ln (1+e_1) + \ln(1+e_2) + \ln(1+e_3)$$

in which Δ is the volume change (positive for volume gains and negative for losses) and e_i is a principal strain. Volume changes based on graptolite strains and using this

relationship lie between 37% and 76% losses, similar to the volume loss determinations based on reduction spots. Thus, an even more precise definition of the finite strain would be constrictional plus a volume loss.

Strains from reduction spots and graptolites agree well, once one takes into account the effects of sedimentary compaction. Graptolites lie in bedding planes and do record the effects of compaction. However, if reduction spots formed early in the depositional history of the Mettawee fm, they would record compaction as well as tectonic strains. We can evaluate these variation on a Flinn diagram (figure 7) which shows that if we add a reasonable amount of compaction, the finite strain recorded by graptolites is essentially coincident with reduction spots and both are strongly indicative of volume losses. of compaction on graptolites (arrow). Note that if a compaction is added on to the graptolite strains they are essentially coincident with reduction spot strains.

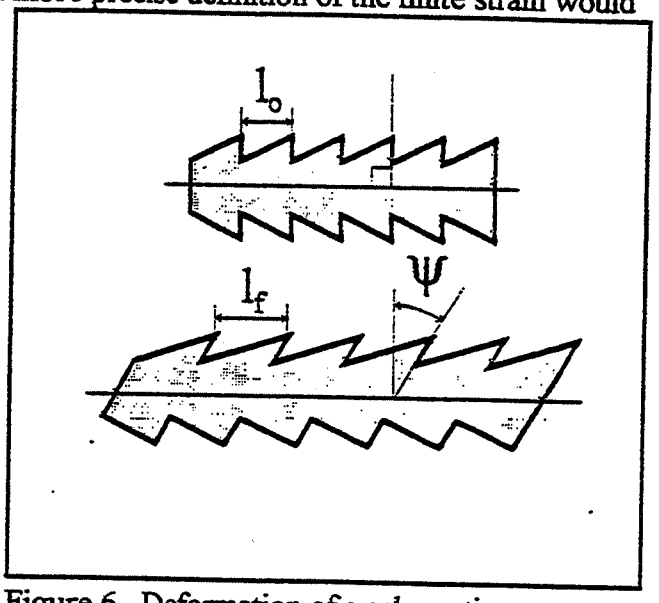

Figure 6. Deformation of a schematic Orthograptus Whitfieldii showing changes in thecal spacing and angle between the thecal aperture and the long axis of the stipe.

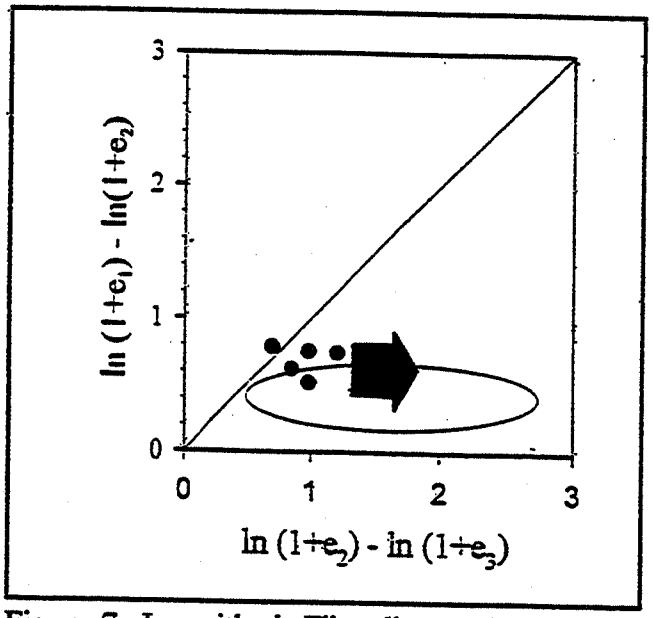

Figure 7. Logarithmic Flinn diagram illustrating the state of strain from graptolites (dots), the range of reduction spots (ellipse) and the effect of adding a compaction on graptolite strain

Other Evidence for Volume Loss. The volume loss determinations for the Taconics agree well with other determinations of volume change from slates (e.g. Wright and Platt, 1982; Beutner and Charles, 1985; Henderson et al, 1986 and Wright and Henderson, 1992; Jenkins, 1988) which typically report between 40% and 60% loss. There is ample evidence that volume loss has affected Taconic slates beyond the finite strain results. Pressure solution was a dominant deformation mechanism during slaty cleavage formation. However, very small volumes of material were redeposited as veins and pressure shadows. Further, whole rock

geochemical studies and micro-scale geochemistry also indicate large volume losses (Goldstein et al, 1995b).

Incremental Strain Results. Whereas the finite strain recorded by graptolites and reduction spots reflects the sum total of all strain events which have affected the Taconics, studies of pyrite framboid and porphyroblast pressure shadows indicate the incremental history of strain. Pickens (1993) studied the porphyroblasts pressure shadows and Cushing and Goldstein (1993) and Chan and Crespi (1995) studies framboid pressure shadows. Unfortunately, all three studies resulted in somewhat different results suggesting that we have yet to fully understand the strain history of the Taconics. Incremental strain analyses of fiber growth around cubic pyrite porphyroblasts (Pickens, 1993) indicate a complex non-coaxial strain history for the slates of the Giddings Brook slice. Pyrite porphyroblasts with associated fibrous strain shadows are locally present throughout the klippe. In some samples, fiber growth parallels changes in cleavage development, providing insight into the transformation of one cleavage into the next. Strain shadow morphology and type vary considerable, but fiber growth can generally be divided into three phases (figure 8). It is important to emphasize, however, that these growth phases should be thought of as continuum of fiber development and not as discontinuous segments. In short, the incremental data demonstrate that the direction of principal extension began parallel to the S_1 foliation (Phase I), rotated (counterclockwise) towards this cleavage (Phase II), and eventually came to lie in the X^Y plane of the S_2 cleavage (Phase III). With the exception of Phase III growth, all increments were plane strain, with no growth in the Y-axis direction. Only the last increment of growth forms a crown, parallel to S_2. These data and observations demonstrate the continuous nature of fabric development during the Taconian deformation.

At one locality with unusually large pyrite framboids, Cushing and Goldstein (1990) described pressure shadows which were composed of segments of long straight fibers, indicating co-axial deformation, separated by short increments of highly curved fibers, indicating a non-coaxial transition between co-axial strain increments. They found four dominant co-axial increments of fiber growth with only minor non-coaxial strains. They concluded that all strain increments were superposed on a pre-existing small fold as none of the fiber segments were rotated between opposing limbs of the fold.

Chan and Crespi (1995) found framboid pressure shadows entirely different from those studies by Cushing and Goldstein (1990) and Pickens (1993). They describe pressure shadows with smoothly curving fibers suggesting a non-coaxial strain history for the Taconics. Below, they argue that these observations can be used to construct a model of S_2 formation as a result of non-coaxial strain. Considering the lack of agreement between the three studies, we suggest that more work needs to be addressed at the strain history of the Taconics.

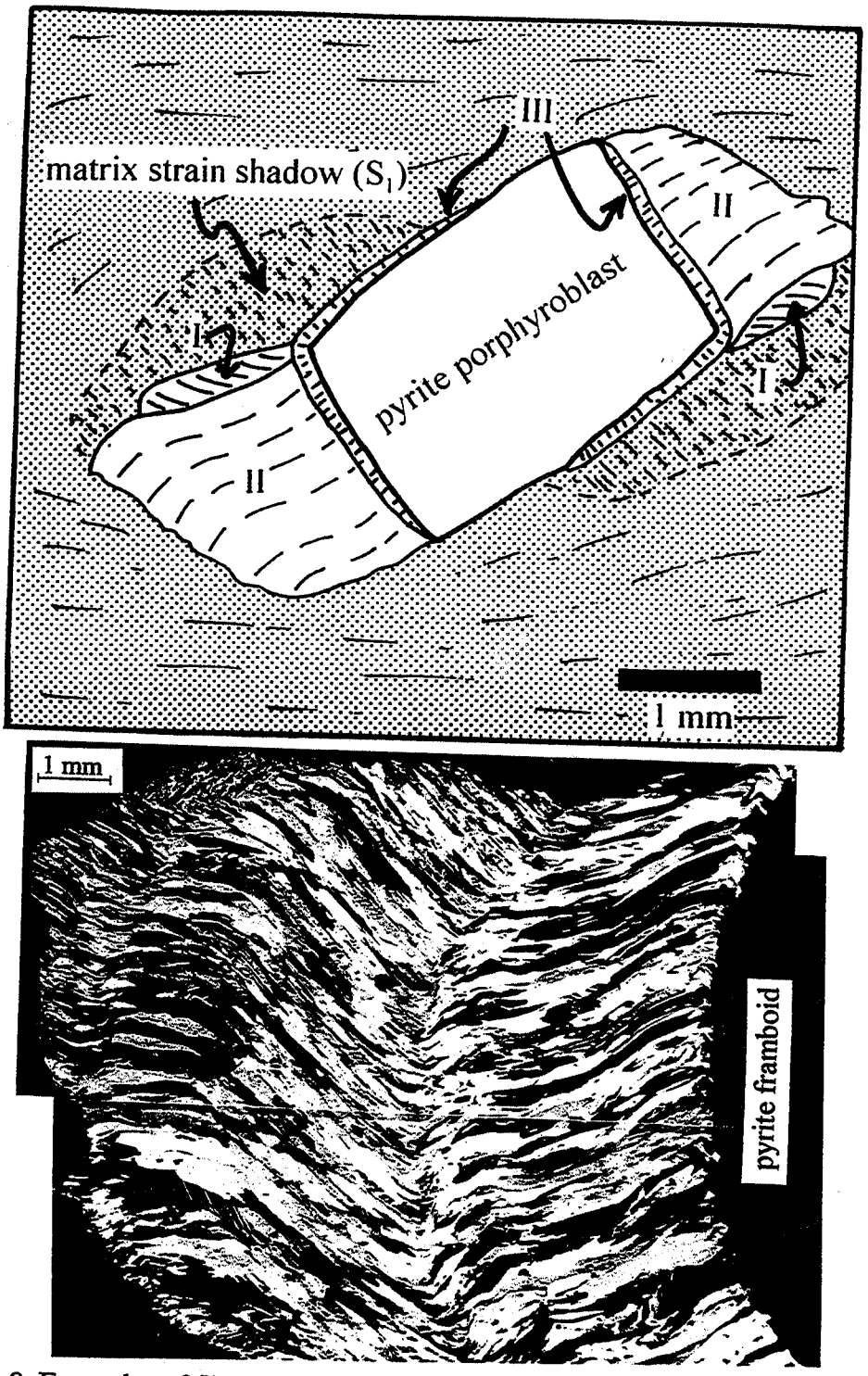

Figure 8. Examples of fibrous pressure shadows developed around pyrite porphyroblasts and framboids. A. Sketch of pyrite porphyroblast showing three stages of fiber growth plus matrix strain shadows which preserve S_1. B. Photograph, in cross polarized light, of large pyrite framboid and pressure shadow showing different stages of largely co-axial fiber growth.

CLEAVAGE DEVELOPMENT
(Chan and Crespi)

At most locations the slaty cleavage observed in the Taconics appears to be an extremely well defined penetrative foliation. In thin section, rather than the single dominant cleavage one might expect, a composite of fabrics can be observed. In the Giddings Brook and Bird Mountain slices, at least two cleavages (S_1 and S_2) can be observed in thin section, with a third (S_3) and fourth (S_4) locally overprinting the earlier fabrics. As discussed below, in the eastern portions of the northern Taconics, S_3 becomes the dominant cleavage and S_2 is barely recognizable.

As one might expect, the slates exhibit a very well developed p- (phyllosilicate), q- (quartz) domainal structure. These domains exist at a variety of scales ranging from single detrital grains to layered concentrations of p and q minerals visible in hand specimen. Where present, the S_1 cleavage is typically at a high angle to S_2, wrapping into the later cleavage along S_2 folia. In examples where this transition in fabrics is preserved, a progressive deformation of S_1, involving grain rotation, strain solution and eventually mineral growth, can be observed.

Development of multiple cleavages Multiple cleavages in rocks are commonly observed in collisional orogenic belts. Studies of their geometry, spatial distribution, and kinematics can contribute significantly to our understanding of the structural processes that occur in orogenic belts and the response of rocks to deformation at depth. The purpose of this section is to provide descriptions of the multiple cleavages observed in the northern Taconic Allochthon and to discuss the kinematics associated with individual cleavages.

Previous work has resulted in the recognition of one locally developed cleavage (S_1) and two regionally developed cleavages (the S_2 slaty cleavage and the S_3 crenulation cleavage of this text) within the northern Taconic Allochthon. The two regionally developed cleavages have been referred to as the Cl1 and Cl2 cleavages (Steuer and Platt, 1981) or, alternatively, the S_2 cleavage and D3-related crenulation cleavage (Bosworth and Rowley, 1984). Recent mapping indicates a regionally developed cleavage (S_4), which was previously unrecognized, is also present in the easternmost part of the Allochthon.

On the basis of the distribution and intensity of the S_2, S_3, and S_4 cleavages, the northern Taconic Allochthon in our study transect (at a latitude of about 43°37'N) can be subdivided into three structural domains. These structural domains are defined from west to east as follows (Fig. 3). Domain A, which extends from the Taconic Frontal thrust to the middle of the Pine Pond thrust sheet, contains a well developed S_2 and a weakly developed S_3. Domain B, which ranges from the middle of the Pine Pond thrust sheet to just east of the peak of Bird Mountain, contains a strongly overprinted S_2, a well developed S_3, and a very weakly developed S_4. Domain C, which extends eastward from domain B, contains a strongly developed S_3 and a moderately to strongly developed S_4. Although the domains are distinct, the domain boundaries represent gradational rather than abrupt changes in the cleavage distribution.

The three regionally developed cleavages differ in geometry, distribution, and intensity and are shown schematically in a geologic cross section across the study transect (Fig. 9). Kinematic studies suggest that S_2 and S_4 developed as a result of west-northwest-directed noncoaxial flow, whereas the flow type for S_3 development is not conclusive based on available data. These conclusions are supported by cleavage-related strain determinations and kinematic indicators associated with individual cleavages. In the following, we describe briefly the morphology, geometry, and distribution of individual cleavages, and we examine kinematic indicators for individual cleavages.

S_1 cleavage. The S_1 cleavage is locally preserved in Domain A of the northern Taconic Allochthon. S_1 is observed to both lie at an angle to bedding and to lie parallel to bedding (Passchier and Urai, 1988). Due to limited preservation, the regional significance of S_1 is unclear although preliminary results suggest that S_1 is related to either early folding or early thrust faulting..

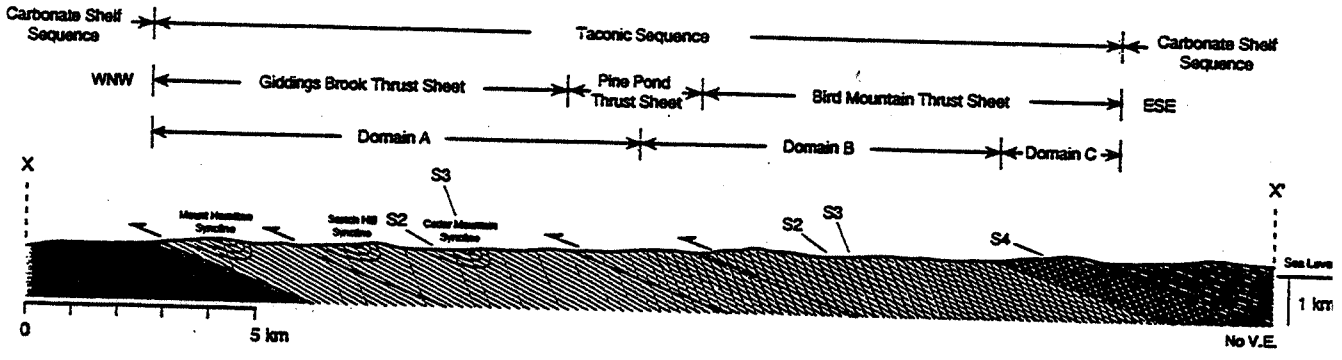

Figure 9. Schematic Cross section of the northern Taconic allochthon showing geometry, intensity and distribution of regionally developed cleavages. Line XX' is shown in fig. 3.

S_2 cleavage. The S_2 cleavage is usually referred to as the regional slaty cleavage because of its pervasiveness within the Taconic Allochthon. In coarse-grained rocks, the S_2 cleavage is a rough to smooth disjunctive cleavage, whereas in finer-grained rocks, it is a fine, continuous cleavage. Textures indicative of dissolution and reprecipitation are commonly observed for S_2. Dissolution is suggested by offset veins and bedding and by truncated detrital grains, whereas reprecipitation is evidenced by strain fringes and veins. The S_2 cleavage is fairly homogeneously distributed and shows minimal variation in orientation across the study transect. In Domains A and B, S_2 strikes on average north-northeast and dips moderately to the east (Fig. 4 and 10). In Domain C, however, measurement of S_2 in the field is not possible because it is strongly overprinted by the S_3 and S_4 cleavages. A graph of the dip of S_2 versus distance from the Taconic Frontal thrust (Fig. 11) shows that the mean dip of S_2 for individual localities ranges only between about 20°E and 40°E. A strong mineral lineation (L_2), which is defined by the alignment of platy minerals (chlorite and white micas) on S_2 surfaces, is a penetrative feature of S_2. This

lineation is generally observable only when a hand lens is used. The mapping of L_2 was conducted largely in Domain A because L_2 is least disturbed by later cleavages in this domain. The results show a consistent east-southeast trend for L_2 (Fig. 10c) similar to that observed by Pickens (1993). Microstructural evidence suggests that S_2 may have

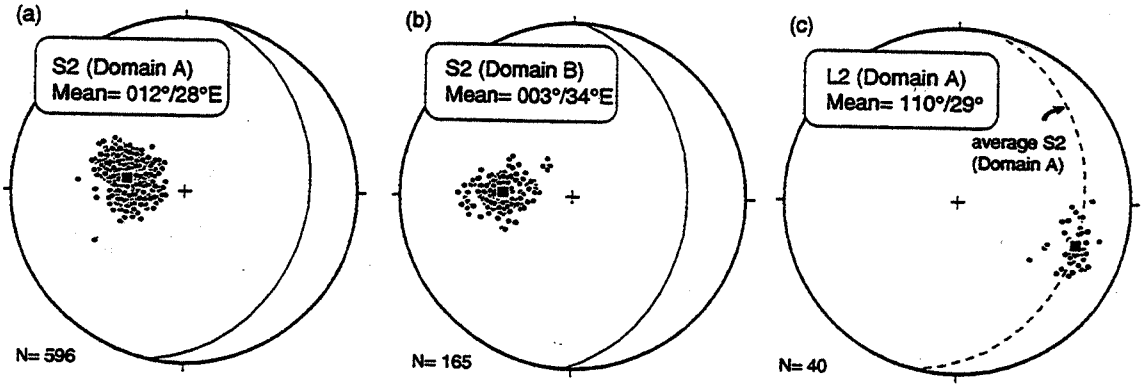

Figure 10. Lower hemisphere, equal area projections of poles to S_2 in domains A and B and L_2 in domain A. Squares show mean orientations.

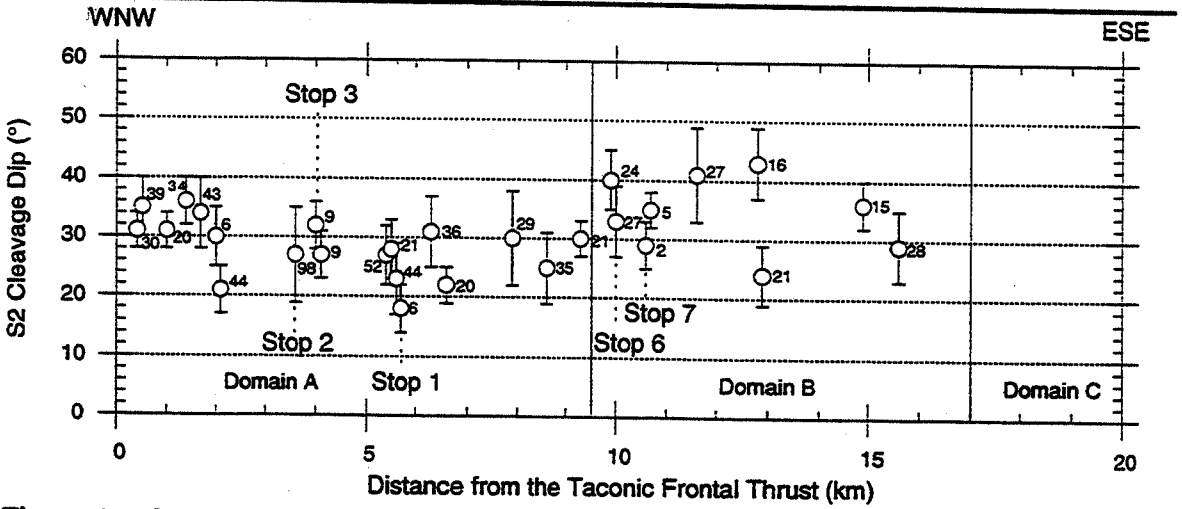

Figure 11. Graph of dip of S_2 versus distance from the taconic frontal thrust. Circles are mean values, lines are one standard deviation and numbers of measurements are shown adjacent to the corresponding symbol.

developed in a noncoaxial flow regime, although this is not a universally held opinion. This evidence comes from kinematic indicators including strain fringes around pyrite framboids and syn-slaty cleavage vein fibers. In addition, basic field relations and evaluation of the relation between S_2 and folding in the core of a regional-scale fold indicates S_2 was superposed on existing asymmetric folds formed by flexural folding.

Evidence for noncoaxial development of S_2: Strain fringes around pyrite framboids Microscale pyrite framboids are commonly observed in the black slates of the northern Taconic Allochthon. The pyrite framboids usually have well defined strain fringes, which provide evidence for the strain history associated with S_2. Several lines of evidence suggest that the strain fringes around the pyrite framboids formed during S_2 development. First, the fibers within the strain fringes show smooth curvature without abrupt changes in orientation or kinks, suggesting that the strain fringes are related to only one deformational event. Second, the S_3 crenulation cleavage is not present or, at most, very poorly developed in the samples used for strain-fringe analysis. Therefore, fiber growth related to the S_3 cleavage is unlikely. Third, the trace of the fibers in the strain fringes in XY sections is parallel to the phyllosilicate lineation in the matrix which formed during S_2 development. This parallelism strongly suggests that the strain fringes are S_2 related.

In XZ sections, the strain fringes around pyrite framboids display smooth clockwise curvature from oldest to youngest fibers when viewed to the NNE, and the youngest fibers, which are adjacent to the framboids, lie at an angle to S_2. The geometry, relative length, and sense of curvature of the fibers in the strain fringes are remarkably consistent across Domain A. On the basis of the similarity in fiber curvature on long and short limbs as well as the similarity in fiber curvature across the ten-kilometer width of Domain A, the fiber geometry is interpreted to reflect a component of top-to-the-west-northwest simple shear. Results of the strain-fringe measurements from five localities in Domain A are shown in Fig. 12, which illustrates the relation between the value determined for the finite elongation using the technique of Durney and Ramsay (1973) and the distance from the Taconic Frontal thrust. The values determined for the finite elongation for the five localities range from 1.1 to 1.4.

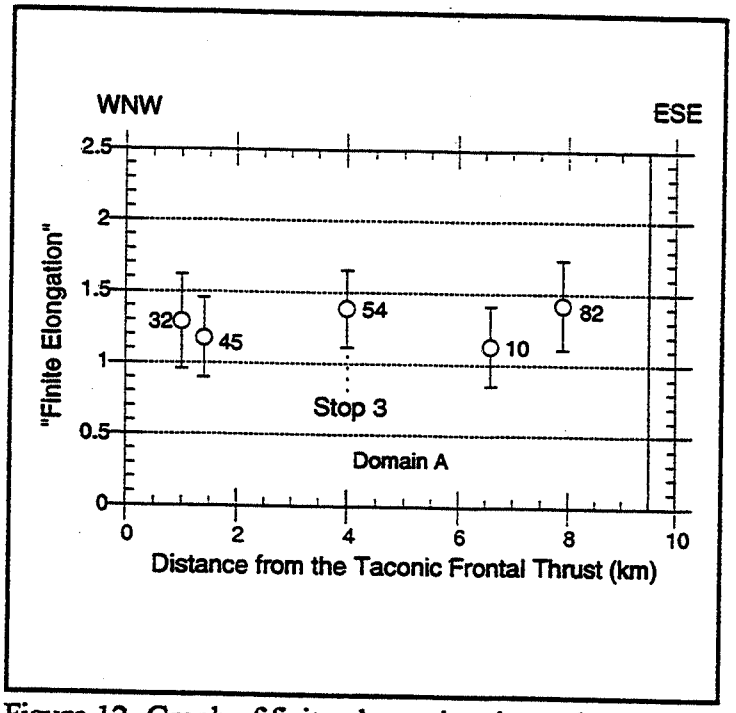

Figure 12. Graph of finite elongation determined from strain fringes around pyrite framboids versus distance from the Taconic frontal thrust. Circles are mean values, error bars are one standard deviation and numbers of measurements are shown.

Evidence for noncoaxial development of S_2: Syn-slaty cleavage vein material. Veins in the northern Taconic Allochthon also record evidence for

top-to-the-west-northwest noncoaxial flow during slaty cleavage development. Exposures of black slate in Domain A, which bear the syn-S_2 strain fringes around pyrite framboids, typically contain two main sets of veins, one striking on average north-south and the other striking on average east-west (Fig. 13). The veins are deformed, being either folded or boudinaged depending on their orientation with respect to S_2. In sandstone and carbonate horizons, the veins lie at approximately right angles to bedding, whereas in slate and silty slate, they lie at low to moderate angles to bedding. Two ages of fill are recognized in the veins that lie in slate and silty slate (Crespi and Chan, 1996). The pre-S_2 vein fill displays blocky as well as fibrous textures and lies within the central part of the veins. Although predominantly composed of calcite, the blocky pre-S_2 vein fill may also contain minor amounts of quartz. In contrast, the syn-S_2 vein fill is composed consistently of fibrous calcite and lies along the margins of the veins. Veins in the north-south striking set more commonly contain both ages of fill, indicating that these veins were preferentially oriented for reactivation during S_2 development.

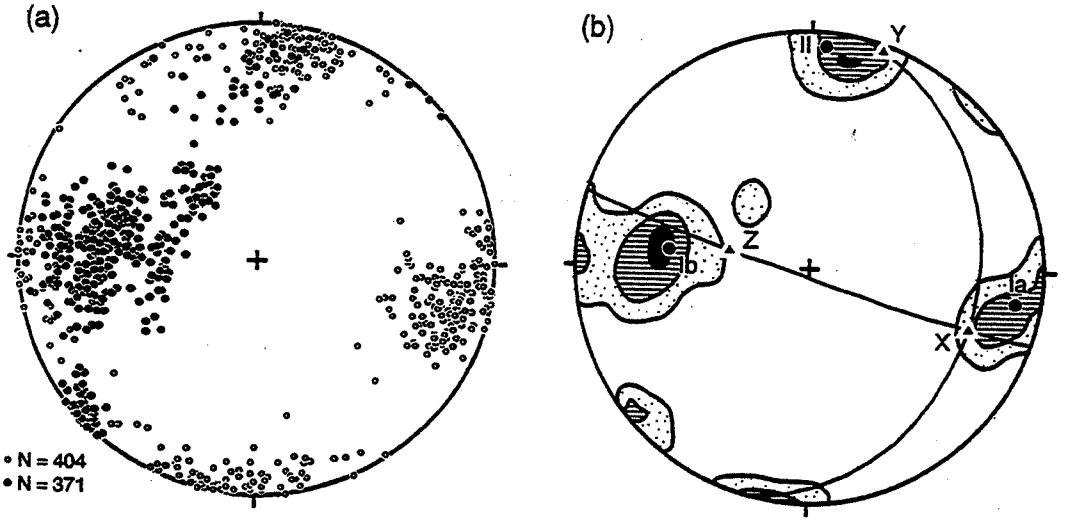

Figure 13. Lower hemisphere, equal area projections of poles to earlt layer-parallel extension veins in domain A. Solid circles are poles to veins in slate. Open circles are poles to veins in limestones and sandstones. X, Y and Z are principal strain axes for S_2 cleavage. Contour interval is 2% per 1% area.

The orientation of the youngest syn-S_2 vein fibers with respect to S_2 can be used to determine whether S_2 formed in a coaxial or noncoaxial flow field. For coaxial flow, the youngest syn-S_2 vein fibers should lie parallel to S_2, whereas for noncoaxial flow, they should lie at an angle to S_2, with the disposition of the fibers to S_2 giving the sense of shear. This assumes the fibers grew parallel to the maximum instantaneous stretching axis, which is likely the case because offset bedding in the wall rock can be connected across a vein by following the trace of the fibers. Because fibers in boudin necks commonly display complex geometries, only non-boudinaged veins in slate or silty slate were analyzed to ensure measurement of the youngest syn-S_2 fibers. Evidence for antitaxial fiber growth

indicates the youngest syn-S_2 vein fibers lie immediately adjacent to the veins walls.

Only four veins were analyzed because of the rarity of non-boudinaged veins in the slate and silty slate. However, in each case, the youngest syn-S_2 vein fibers are at an angle to S_2 such that the fibers lie clockwise from S_2 when viewed to the north-northeast; mean angles range from 26° to 34°. Like the results from the analysis of the syn-S_2 strain fringes around pyrite framboids, these results are consistent with top-to-the-west-northwest noncoaxial flow during S_2 development.

Relation of slaty cleavage development to folding. The relation between slaty cleavage development and folding in Domain A was evaluated at an outcrop of the Scotch Hill syncline. The outcrop is unusual because it exposes the core of a regional-scale fold and because it contains small-scale structures, in particular veins, that may be related to fold development. On the subvertical short limb of the syncline, en echelon, sigmoidal veins are "Z"-shaped when viewed to the north-northeast, indicating east-side-down displacement parallel to bedding. On the gently east-dipping long limb, sigmoidal veins are "S"-shaped when viewed to the north-northeast, indicating top-to-the-west displacement parallel to bedding. These observations suggest that this asymmetric fold formed by flexural folding and that pinning was along the hinge, at least from the time of initial formation of the veins. Thus, if hinge migration was involved in the development of fold asymmetry, it must have occurred early in the history of folding. Bedding-parallel veins at the outcrop are also consistent with flexural folding and a pinned hinge. The two bedding-parallel veins lie on the long limb of the fold and die out at similar distances from the hinge. In addition, inclined layer-silicate microstructures (Crespi, 1993) in the veins indicate top-to-the-west displacement. The absence of bedding-parallel veins on the short limb of the fold may be a result of the outcrop geometry, which preserves a greater length of the long limb.

The preceding observations together with the results of the strain-fringe and vein-fiber analyses imply that the slaty cleavage is not related to folding but was superposed on the fold shapes that developed as a result of the flexural folding process.

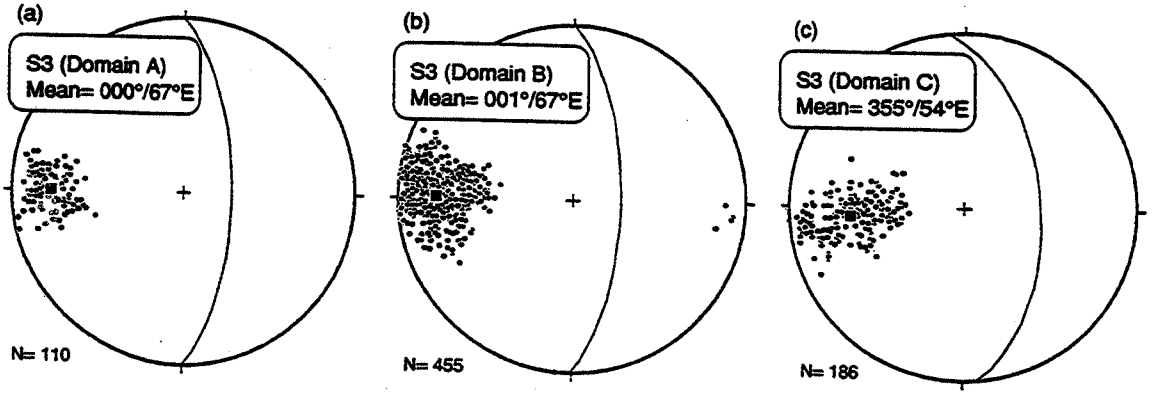

Figure 14. Lower hemisphere, equal-area projections of poles to S_3 in domains A, B and C. Squares show mean orientations.

Although data were not obtained for the short limb of the Scotch Hill syncline because of the lack of suitable markers, strain-fringe and vein-fiber data for the short limb of the Mount Hamilton syncline record top-to-the-west-northwest displacement, which is inconsistent with flexural folding and pinning along the fold hinge. The isoclinal geometry of the folds in the northern Taconic Allochthon, therefore, appears to be a result of flattening of flexural folds during regional-scale, top-to-the-west-northwest noncoaxial flow and slaty cleavage development.

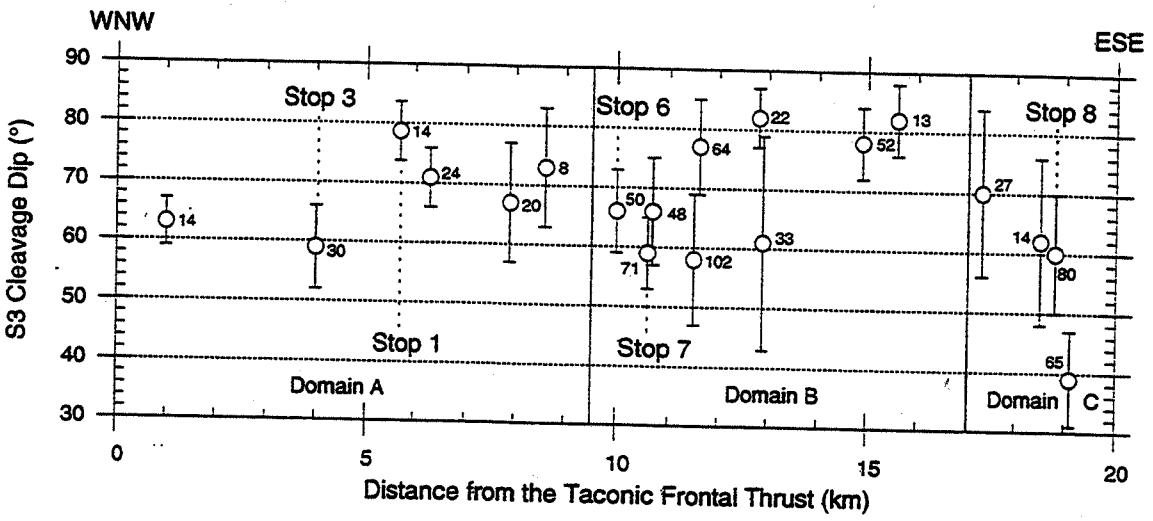

Figure 15. Graph of dip of S_3 versus distance from the Taconic frontal thrust. Circles are mean values, error bars are one standard deviation and numbers of measurements are shown adjacent to symbols.

S_3 cleavage. The S_3 cleavage is a crenulation cleavage and is dominated by pressure solution. The S_3 cleavage is mainly a zonal crenulation cleavage characterized by gradational boundaries between the cleavage and microlithon domains, although it also appears as a discrete crenulation cleavage characterized by abrupt boundaries between microlithon domains. From west to east across the study transect, the spacing of the S_3 cleavage decreases, and the amount of crystallization of new micas along cleavage domains increases. The S_3 cleavage is only locally present in

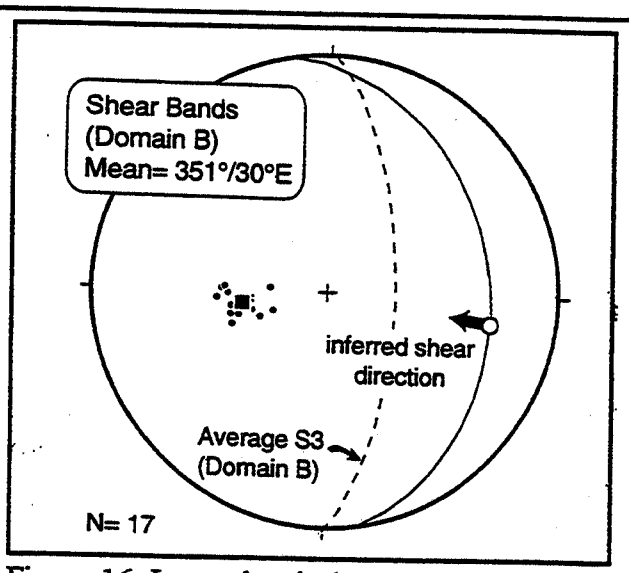

Figure 16. Lower hemisphere, equal area projection of poles to shear bands in domain B. Square is mean orientation

Domain A and becomes more pervasive in Domains B and C. S_3 strikes on average north and dips steeply to the east (Fig. 14). A graph of the dip of S_3 versus distance from the Taconic Frontal thrust (Fig. 15) shows that the mean dip of S_3 ranges only between about 60°E and 80°E. Although the dip of the S_3 cleavage is relatively constant across the study transect in Domain B, it decreases systematically from west to east in Domain C. Shallowly east-dipping extensional shear bands are locally present in Domain B. These shear bands are commonly traceable for less than one meter and have a spacing of about one decimeter to a few decimeters. All the observed extensional shear bands truncate S_3 in their centers; however, their tips curve smoothly into near parallelism with S_3. This suggests that these extensional shear bands were developed late in the history of S_3. The geometry of the extensional shear bands gives a top-to-the-west-northwest sense of shear (Fig. 16).

S_4 cleavage. The S_4 cleavage is a previously unrecognized cleavage that crosscuts S_3. Similar to S_3, pressure solution is the dominant deformation mechanism, although S_4 shows stronger crystallization of new micas along the cleavage domains. The S_4 cleavage domains are dominated by muscovite and chlorite; minor minerals include quartz, chloritoid, albite, paragonite, and rutile. The thickness of the cleavage-domain phyllosilicate grains ranges from about 10 to 100 microns, which is significantly greater than that observed for the phyllosilicate grains in the cleavage domains of S_2 and S_3. The S_4 microlithon domains contain dominantly quartz, albite, muscovite, chlorite, and rutile.

The S_4 cleavage is weakly developed in the easternmost part of Domain B; however, it is pervasively developed in Domain C. The intensity of the S_4 cleavage increases from west to east. S_4 strikes on average north and dips gently to the east (Fig. 17a). Mesoscopically, S_4 is characteristically lustrous and has a mineral lineation (L_4)

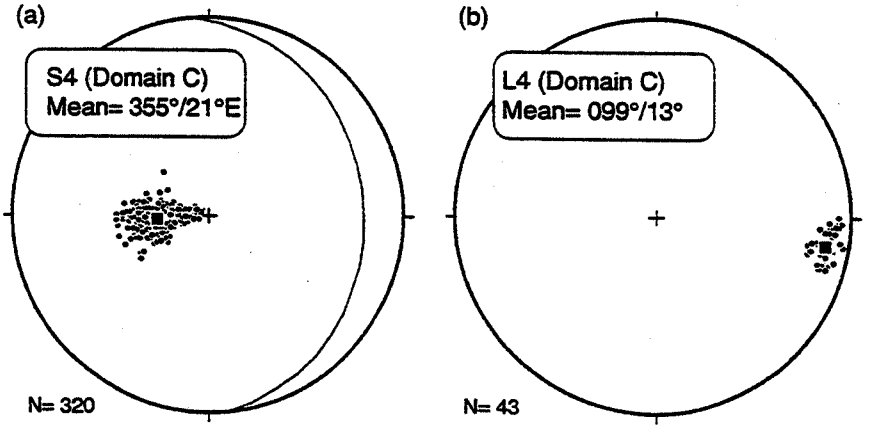

Figure 17. Lower hemisphere, equal area projections of poles to S4 and L4 in domain C. Squares are mean orientations.

which is readily observed and measured in the field (Fig. 17b). A graph of the dip of S_4 versus distance from the Taconic Frontal thrust shows that the mean dip of S_4 gradually decreases from about 30°E to 10°E from west to east (Fig. 18).

The microlithon domains of S_4 commonly contain syntectonic albite porphyroblasts. These albite porphyroblasts generally have a long dimension less than 0.25 mm and a short dimension less than 0.12 mm. The porphyroblasts are characterized by inclusion-rich albite cores and inclusion-free albite overgrowths. The kinematics of the S_4 cleavage is indicated by the asymmetry of the portion of the albite overgrowths that is related to the development of S_4. The asymmetry of the albite overgrowths suggests that the S_4 cleavage developed noncoaxially with a top-to-the-west-northwest sense of shear.

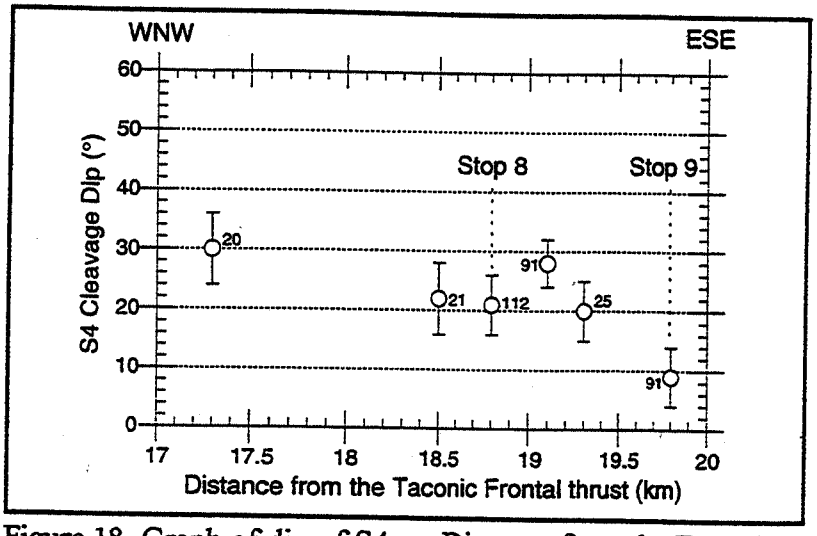

Figure 18. Graph of dip of S4 vs. Distance from the Taconic frontal thrust. Circles are mean values, error bars are one standard deviation and numbers of measurements are shown.

Discussion. An important question is the age and tectonic significance of the S_2, S_3, and S_4 cleavages. Harper (1968) dated six samples of slate and phyllite from the northern Taconic Allochthon using conventional K-Ar whole-rock methodology. His results were recalculated by Sutter et al. (1985), who applied newer constants for the K-Ar radiometric system. The recalculated apparent ages range from 468±8 to 381±8 Ma, i.e., from middle Ordovician to middle Devonian. Although Sutter et al. (1985) argue against a possible Acadian age for the cleavages in the Taconic Allochthon, the six apparent ages correspond very well with the deformational complexity at Harper's sample locations. The two oldest ages (468±8, 453±8 Ma) are from locations where S_2 is dominant, and the two youngest ages (394±8, 381±8 Ma) are from locations where the rocks are severely overprinted by S_3. Because the peak temperature for the formation of slate and phyllite is very likely below the closure temperature for argon retention in white mica, the radiometric ages of white mica growing in cleavage domains may represent the formation age of the white mica, and, thus, the cleavage. For samples with more than one cleavage, the apparent age may represent a mixed age such that the obtained age is a maximum estimate for the youngest cleavage generation in the sample. Therefore, the results of Harper's dating suggest that S_2 is Taconic in age, whereas S_3 and S_4 are younger and possibly Acadian in age.

The available radiometric ages, however, are open to question because of uncertainty with respect to the assumption that the white mica growing in the cleavage domains is the main potassium-bearing phase in the slate and phyllite. For example,

detrital mica, detrital potassium feldspar, and diagenetic mica are all possible potassium-bearing minerals in these rocks. Thus, a better dating technique should be applied. We (Chan and Crespi) are currently dating samples in which a single cleavage (either S_2, S_3, or S_4) is dominant using the laser probe ^{40}Ar-^{39}Ar method. This advanced dating method will help in constraining the age of specific cleavage domains in a slate or phyllite with good precision, and the results should provide a better estimation of the cleavage ages. Samples from the study transect as well as Harper's original sample locations are included in this geochronologic study.

In addition to the available geochronologic data, differences in orientation data for S_2 and S_3/S_4 also suggest that S_2 and S_3/S_4 may have developed during separate tectonic events. First, S_2 strikes on average 012^0 (Domain A), whereas S_3 and S_4 strike on average 001^0 (Domain B) and 355^0 (Domain C), respectively. Second, L_2 trends on average 110^0, whereas L_4 trends on average 099^0. (L_3, which is less well developed than L_4, trends about parallel to L_4.) Third, S_2 is relatively homogeneous in terms of cleavage spacing, whereas the spacing of S_3 and S_4 decreases from west to east. Although not conclusive, these differences are consistent with at least two tectonic events for S_2 and S_3/S_4. It remains unclear, however, whether there is a significant time gap between the development of S_3 and S_4 without additional radiometric ages.

S_2 is interpreted to have formed during the WNW-directed emplacement of the northern Taconic Allochthon. In addition, structural data for S_2 can be explained relatively easily using the cleavage trajectory model proposed by Sanderson (1982), which has been applied to a number of other slate belts (e.g., Gray and Willman, 1991; Sanderson, 1979; Tillman and Byrne, 1995). In this model, cleavage curves asymptotically toward the base of a regional-scale thrust sheet (Fig. 19). In the upper portion of the thrust sheet, cleavage development is characterized by coaxial flow, whereas in the lower portion, cleavage development is characterized by noncoaxial flow. If Sanderson's cleavage trajectory model applies, the kinematics and geometry of S_2 indicate the study transect lies within the lower portion of a thrust sheet and at the same

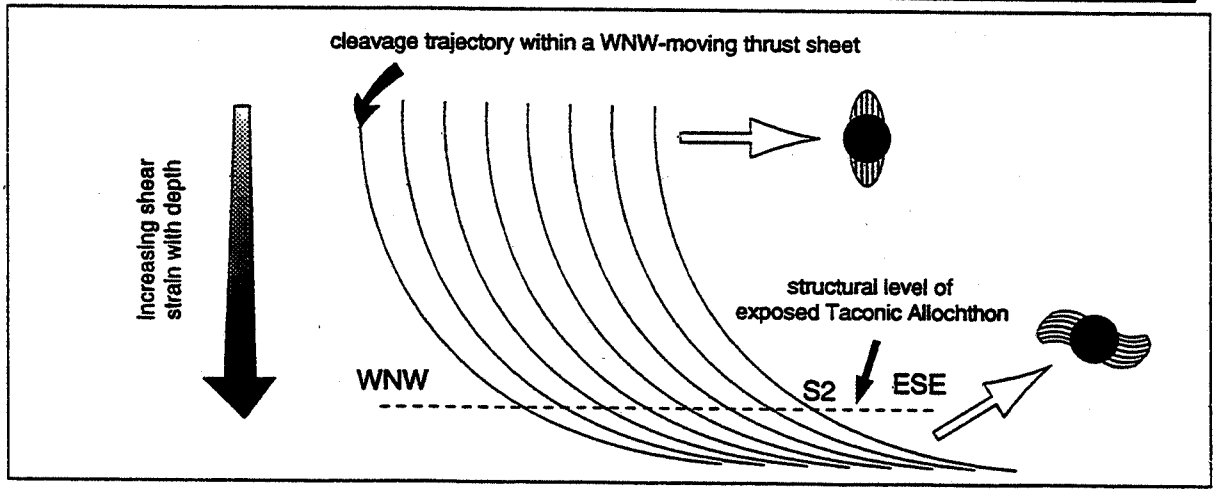

Figure 19. Schematic diagram showing cleavage-trajectory model of the interpretation of S_2.

structural level. This interpretation is suggested by (1) the lack of variation in S_2 orientation, (2) the lack of variation in strain magnitude as determined from syn-S_2 strain fringes around pyrite framboids, and (3) the consistent curvature of the syn-S_2 strain fringes.

In contrast to S_2, the tectonic significance of S_3 is less straightforward because of the lack of reliable microscale kinematic indicators for S_3. Based on available structural data related to S_3, possible tectonic interpretations for S_3 include (1) development of S_3 as an axial planar cleavage in a coaxial flow during formation of a regional-scale fold and (2) development of S_3 as a footwall cleavage in a noncoaxial flow during a regional-scale thrusting event. The increase in intensity of S_3 from west to east, which suggests an increase in strain magnitude, is consistent with both tectonic interpretations (i.e., an increase in strain from an upright to an overturned limb and an increase in strain toward a thrust plane). The late-S_3 extensional shear bands dip in only one direction, suggesting S_3 may have formed in a noncoaxial flow. However, because the extensional shear bands are only found at one locality, they may not be representative for the study transect. It is also possible that S_3 formed in a coaxial flow with a possible post-S_3 noncoaxial event being responsible for the shear bands.

Insight into the tectonic significance of S_4 can be gained by comparing the geometric, morphologic, and kinematic characteristics of S_4 with those of S_2 and S_3. First, S_4 dips relatively gently to the east in contrast to the steeply dipping S_3. Second, S_4 shows a rapid transition from weakly to strongly developed in contrast to the relatively gradual transition for S_3 and the homogeneously developed S_2. Third, the stretching lineation on S_4 is very strong. Fourth, S_4 contains microscale albite porphyroblasts, which indicate S_4 developed in a noncoaxial flow. Together, these observations suggest that S_4 formed in a shear zone that is characterized by enhanced noncoaxial flow and high strain magnitude. In such a zone, the angle between the shear plane and the developed cleavage is very low. Thus, the development of S_4 may have been related to motion along a regional-scale, WNW-directed thrust.

References

Beutner, E. C. & Charles, E. G. 1985. Large volume loss during cleavage formation, Hamburg sequence, Pennsylvania. Geology, v. 13, p. 803-805.

Bird, J.M. and Dewey, J.F. 1970. Lithosphere plate-continental margin tectonics and the evolution of the Appalachian orogen. Geol. Soc. Am. Bull., v. 81, p. 1031-1060.

Bosworth, W., and D. B. Rowley, 1984, Early obduction-related deformation features of the Taconic allochthon: analogy with structures observed in modern trench environments: Geological Society of America Bulletin, v. 95, p. 559-567.

Crespi, J. M., 1993, Inclined layer-silicate microstructures and their use as a sense-of-slip indicator for brittle fault zones: Journal of Structural Geology, v. 5, p. 233-238.

Crespi, J. M., and Y.-C. Chan, 1996, Vein reactivation and some complex vein intersection geometries: Journal of Structural Geology, v.18, p. 933-939.

Cushing, J. & Goldstein, A. G. 1990. Strain history of a mesoscale similar fold in Taconic slates, western Vermont (abstr.). Geol. Soc. America Abstracts with Programs., v. 22, p.10.

Fisher, D. W., Y. W. Isachsen, and L. V. Rickard, 1970, Geologic map of New York State: New York State museum and Science Service Map and Chart Series 15.

Goldstein, A. , Pickens, J., Klepeis, K. and Linn, F., 1995a. Finite strain heterogeneity and volume loss in slates of the Taconic Allochthon, Vermont, U.S.A. *J. Struct. Geol.*, v.17, p. 1207-1216.

Goldstein, A., Brauer, N. and Pickens, J., 1995b, Strain shadows in slate: Windows for studying compositional changes accompanying deformation. Geol. Soc. Am. Abstracts with Programs, v. 27, p. A72.

Goldstein, A., Knight, J. and Kimball, K., in press, Deformed graptolites, finite strain and volume loss during cleavage formation in rocks of the Taconic slate belt, New York and Vermont, USA, Jour. Str. Geol.

Gray, D. R., and C. E. Willman, 1991, Thrust-related strain gradients and thrusting mechanisms in a chevron-folded sequence, southeastern Australia: Journal of Structural Geology, v. 13, p. 691-710.

Harper, C. T., 1968, Isotopic ages from the Appalachians and their tectonic significance: Canadian Journal of Earth Sciences, v. 5, p.49-59.

Henderson, J. R., Wright, T. O. & Henderson M. N. 1986. A history of cleavage and folding: an example from the Goldenville Formation, Nova Scotia. J. Struct. Geol., v. 97, p. 1354-1366.

Hoak, T. 1992. Strain analysis, slaty cleavage and thrusting in the Taconic slate belt, west-central Vermont. Northeastern Geol., v. 14, p. 7-14.

Jenkins, C.J. 1987. The Ordovician graptoloid Didymograptus murchisoni in South Walse and its use in three dimensional absolute strain analysis. Trans. R. Soc. Edinb. Earth Sci., v. 78, p. 105-114.

Passchier, C. W., and J. L. Urai, 1988, Vorticity and strain analysis using Mohr diagrams: Journal of Structural Geology, v. 10, p. 755-763.

Pickens, J. 1993. Strain partitioning and cleavage formation in the Mettawee slates of the Taconic allochthon. M.S. Thesis, University of Massachusetts.

Rowley D. B., Kidd, W. S. F., & Delano, L. L. 1979. Detailed stratigraphic and structural features of the Giddings Brook slice of the Taconic allochthon in the Granville area. In: New York State Geological Association and NEIGC Guidebook of Field Trips (edited by Friedman, G. M.). Rensselar Polytechnic Institute, Troy, New York, 186-242.

Rowley, D. B & Kidd, W. S. F. 1981. Stratigraphic relationships and detrital composition of the Medial Ordovician Flysch of western New England; implications for the tectonic evolution of the Taconic Orogeny. J. Geol., v. 89, 199-218.

Sanderson, D. J., 1979, The transition from upright to recumbent folding in the Variscan fold belt of southwest England: A model based on the kinematics of simple shear: Journal of Structural Geology, v. 1, p. 101-109.

Sanderson, D. J., 1982, Models of strain variation in nappes and thrust sheets: a review: Tectonophysics, v. 88, p. 201-233.

Stanley, R. S. & Ratcliffe, N. M. 1985. Tectonic Synthesis of the Taconian Orogeny in Western New England. Bull. geol. Soc. Am., v. 96, 1227-1250.

Steuer, M. R., and L. B. Platt, 1981, A structure section in eastern New York showing variation in style of deformation across the Taconic allochthon: Northeastern Geology, v. 3, p. 134-137.

Sutter, J. F., N. M. Ratcliffe, and S. B. Mukasa, 1985, Ar40/Ar39 and K-Ar data bearing on the metamorphic and tectonic history of western New England: Geological Society of America Bulletin, v. 96, p. 123-136.

Tillman, K. S., and T. B. Byrne, 1995, Kinematic analysis of the Taiwan Slate Belt: Tectonics, v. 14, p. 322-341.

Wood, D. S. 1974. Current views on the development of slaty cleavage. Annual Reviews Earth and Planetary Sciences, v. 2, p. 369-401.

Wright, T. O. & Henderson, J. R. 1992. Volume loss during cleavage formation in the Meguma Group, Nova Scotia, Canada. J. Struct. Geol., v. 14, p. 281-290.

Wright, T. O. & Platt, L. B. 1982. Pressure dissolution and cleavage in the Martinsburg shale. Am. Jour. Sci., v. 282, p. 122-135.

Road Log

Directions from Pico

Meet at parking area of Pico. Drive east on Rt. 4 towards Rutland.
Intersection of Rt. 4 and Rt. 7. Turn Left to stay on Rt. 4 east.
Turn right to remain on Rt. 4.
Exit to Rt. 30 south. Drive to Intersection with with Rt. 4A. Turn right onto Rt. 4A at Castleton Corners.

Mileage begins at Intersection of Rt 30 with Rt 4A

1.2	Turn right (west) onto Creek Road. Roadcuts of Mettawee fm. On the left as you drive along the west shore of Lake Bomoseen.
5.1	Entrance to Lake Bomoseen State park on right; road curves sharply to left...continue straight onto dirt road which follows lake shore. Continue until road ends.
6.4	Park so as to not block in other drivers or residents.

STOP 1. Cedar Point Quarry

The Cedar Point quarry lies on the hinge of a first-order syncline developed in the Mettawee fm. This structure, typical of the Taconics (fig. 20), is extremely well displayed within the quarry. As one walks up into the quarry, a folded bedding surface is seen on the right which defines the hinge of this syncline. Along this surface one can see bedding cleavage intersections which parallel the fold axis. Within the quarry itself the same hinge is well displayed and the axial plane orientation of the slaty cleavage (S_2) can be seen. This site is one which was used for the study of reduction spots (Goldstein er al, 1995a) and the spots are easily seen here. Note that some spots are nearly perfect ellipsoids with their XY planes parallel to the cleavage. Other spots are irregular and were not measured for strain analyses. One can also observed pyrite porphyroblasts with pressure shadows and S_3 crenulation cleavage at this locality.

	Turn around and retrace the route to Creek Road.
7.6	Turn right onto Creek Road
7.7	Creek Road curves to left, continue straight onto dirt road.
7.8	Turn left onto another dirt road (Moscow Road ?) Park along right side of road so as to not block traffic. The stop lies at the intersection of the dirt road and Scotch Hill Rd.

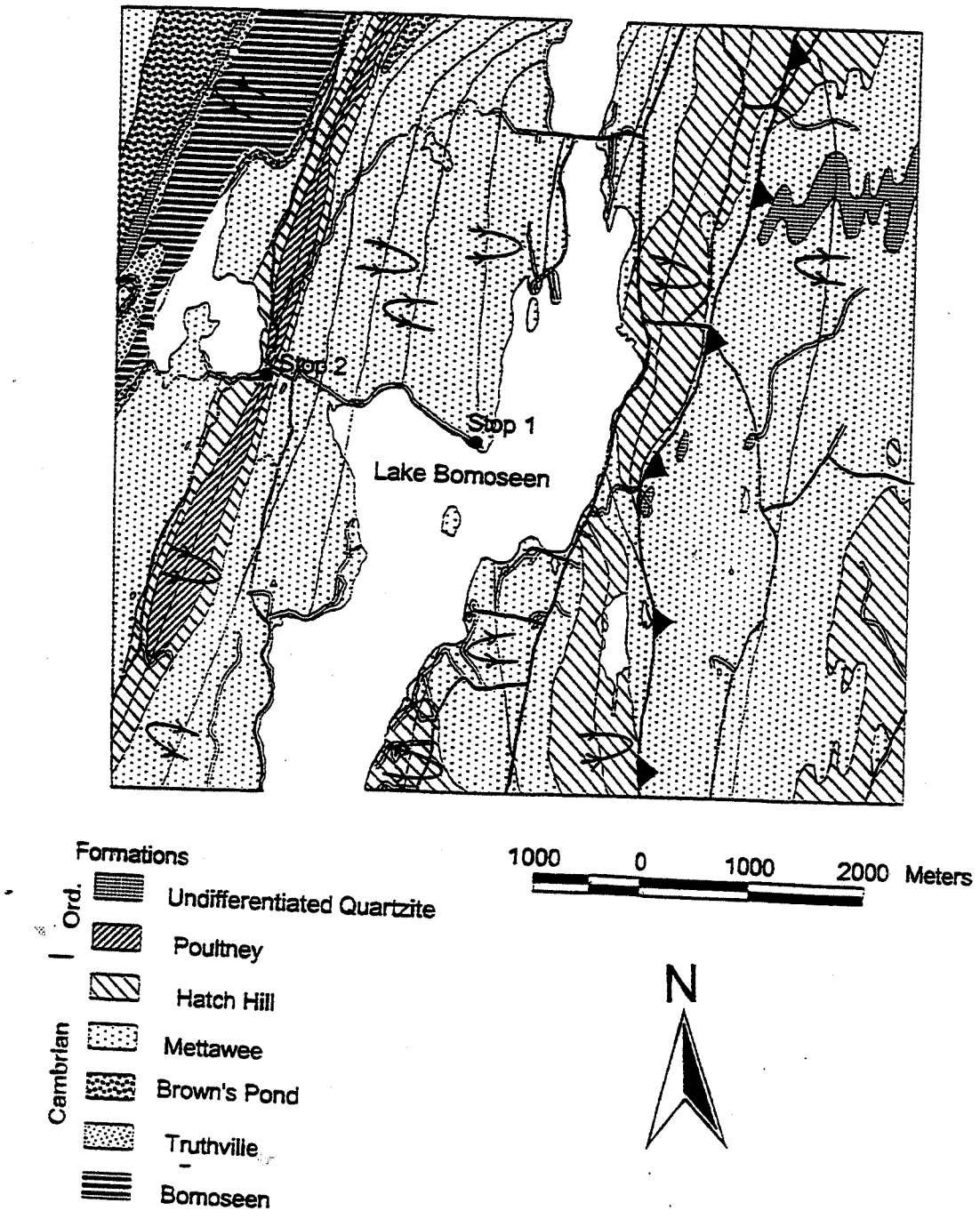

Figure 20. Geologic map of the southern portion of the Bomoseen 7 ½ minute Quadrangle showing locations of stops 1 and 2.

STOP 2 Scotch Hill Syncline

The purpose of this stop is to show some aspects of the pre-slaty cleavage deformation history of the Taconic sequence. In particular, we will examine two generations of veins, one related to early, layer-parallel extension and the other related to fold development, and we will evaluate evidence for fold development by flexural folding. The locality exposes the core of the Scotch Hill syncline, a regional-scale, west-vergent asymmetric fold. The strata at this location are within the Poultney fm. and are composed of cm. scale alternating layers of black and gray silty slate and brown-weathering dolomitic meta-arenites, which are bedded at the meter scale.

Two sets of veins can be observed in the lowermost slate horizon. The older set, which formed during a period of early, pre-folding, layer-parallel extension, appears to be approximately parallel to the slaty cleavage on the profile plane of the fold. Bedding-parallel surfaces show, however, that the veins lie at an angle to the slaty cleavage and are noncoaxial with the fold. Good three-dimensional exposures of the veins are visible on the short limb of the fold. These pre-folding veins also show little variation in orientation across the fold, being essentially parallel on the long and short limbs. This results from a combination of rotation of the fold limbs and distributed shear parallel to layering in the siltstone during flexural folding. Cross-cutting relations between the early, pre-folding, layer-parallel extension veins and a set of younger, en echelon, sigmoidal veins are visible on both the long and short limbs of the fold. The en echelon, sigmoidal veins are coaxial with the fold and formed during fold development. On the short limb, the veins are "Z"-shaped, indicating east-side-down sense of shear along bedding. Veins that display a straightforward sigmoidal geometry on the long limb are "S"-shaped, indicating top-to-the-west sense of shear along bedding. These veins provide evidence for distributed shear along bedding during flexural folding and indicate pinning was along the fold hinge.

Another set of veins, consisting of two bedding-parallel veins, is present in the exposure and provides evidence for discontinuous shear parallel to bedding during flexural folding. These veins lie in the center of the two dolomite units and only exist on the long limb of the fold.

Finally, the approximately axial planar nature of the slaty cleavage (S_2) is well shown at this locality. S_2 is inferred to have been superposed on the fold subsequent to vein development and flexural folding.

7.8	Turn right onto Scotch Hill Road
11.8	Intersection with Rt. 4; park along right side of road. Walk down exit ramp towards Rt. 4 east.

STOP 3

The purpose of this stop is to show meso- and microscale structures that are characteristic of Domain A and to present evidence for top-to-the-west-northwest

noncoaxial flow during slaty cleavage (S_2) development. In addition, some aspects of the history of vein development will be noted.

The locality exposes the long limb of the Scotch Hill syncline, and the strata are composed of slate and silty slate interbedded with limestone and limestone conglomerate. As is typical of Domain A, the slaty cleavage (S_2) is the main cleavage at this locality, and it dips on average 30¡ to the east-southeast. A crenulation cleavage, which dips on average 59¡ to the east, is also locally present. Although not visible in the field, a penetrative mineral lineation (L2) defined by the preferred orientation of phyllosilicates is present on the S_2 surfaces. Also prominent at the exposure are early layer-parallel extension veins which have been variably reactivated during slaty cleavage development. The veins, which are primarily composed of calcite, lie in two main sets, the veins in one striking on average north-south and the veins in the other striking on average east-west. Good examples of boudinaged veins belonging to the north-south striking set and folded veins belonging to the east-west striking set are present within the slate layers throughout the exposure. Pre-S_2 and syn-S_2 vein fill can be discerned for some of the veins in the field using a hand lens, although microscale observations are generally needed to confirm the age of the vein fill. Reactivation of the veins during S_2 development has resulted in complex vein intersection geometries in the slate layers (Crespi and Chan, 1996); some good examples are visible on the top of the exposure between Rte. 4 and the exit ramp. Finally, syn-S_2 strain fringes from this locality provide evidence for top-to-the-west-northwest noncoaxial flow during S_2 development.

	Continue straight on Scotch Hill Rd.
12.3	Flashing light; continue straight towards Fair Haven, Vt. Drive through town of Fair Haven.
13.0	Turn left onto River St.
14.1	Turn right onto Evergreen Rd. Quarries in Mettawee Fm. On left. These are active quarries and should not be entered without permission.
15.3	Road curves sharply to left, park on Sawmill Rd. which continues straight. Walk back to Evergreen Rd. And follow path to right of pile of rock dust. Follow sketch map to find the quarry which is the next stop. Note: there are many paths and quarries in this area and it is easy to get lost, even for a geologist !

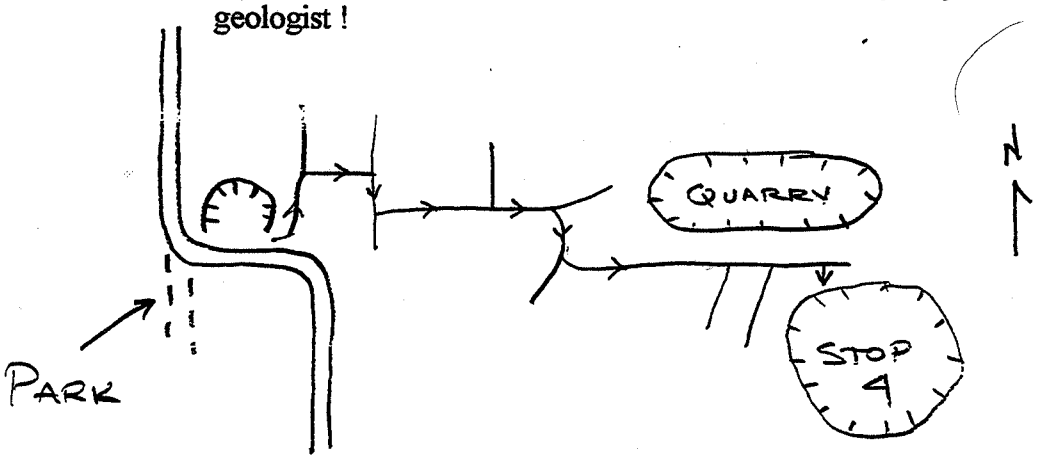

STOP 4 : LUNCH

This quarry is located on the upright limb of one of the isoclinal folds and displays parallel bedding and cleavage. Our purpose here is to examine another more reduction spots as well as pyrite porphyroblasts with pressure shadows and late stage faulting and veining. The quarry sits astride the contact between the Mettawee and Hatch Hill (black, rusty-weathering slate) formations and the contact is exposed on the upper bench of the quarry. Veining is abundant as large sigmoidal veins filling late brittle faults and as veins localized within meta-arenites in the hatch Hill fm. The sigmoidal veins fill early faults whcih were then further deformed in a ductile shear environment to yield the sigmoidal shape.

This site was also used of an oxygen isotope study. Early (folded) quartz veins, syn-tectonic quartz mineralization in boudin necks and the late veins were all analyzed for $\delta^{18}O$ in the stable isotope lab at the University of Wisconsin. All the isotopic ratios are nearly identical varying between 18.57 and 19.10. Further, no zoning of $\delta^{18}O$ within single veins was observed. We interpret these results as indicating that fluid flow was pervasive and intragranular resulting in homogenization of oxygen isotopes between fluids and rock.

	Continue south on Evergreen Rd.
16.4	Turn right onto Saltis Rd. The quarries near this intersection take stone from the Mettawee Fm., are active and you must receive permission to enter them.
16.6	Turn right onto Bolger Rd.
18.2	Turn left onto Rt. 22A
28.9	Turn left onto Rt. 24; Middle Granville. Cross steel deck bridge
29.0	Turn left onto Depot Rd.
29.8	Turn left onto Stoddard Rd.
30.3	Park on right side of road.

STOP 5 Deformed Graptolites

This stop exposes the principal graptolite-bearing stratigraphic unit within the Taconics. Rowley et al (1978) defined this rusty weathering black slate at the top of the Mt. Merino fm and named it the Stoddard Rd. Member. Because it occurs at the very top of the Taconic stratigraphy, the Stoddard Rd. Member is only found in the deepest synclines, which is the structural setting for this stop. The outcrop located on the road lies on the limb of this syncline as bedding and cleavage are parallel (note: bedding can be defined as the plane on which graptolites lie. Along the road, graptolites lie on cleavage indicating bedding-cleavage parallelism). Three species were used for strain measurement: *Orthograptus Calcaratus, Orthograptus Whitfieldii and Climacograptus Bicornis*. All three species are abundant, are easily recognized and have constant thecal spacing in the

undeformed state. For this site, graptolite measurement indicates that X is 32% elongation and Y is 40% shortening.

Across the road in the beaver pond is another exposure which lies on the hinge of the syncline. Bedding-cleavage intersection varies from 60° to 90°. The same species can be found in these rocks and their measurement indicates 60% shortening perpendicular to cleavage.

	Turn around and retrace the route.
30.9	Turn right onto Depot Rd.
31.6	Turn right onto Rt. 24, cross steel deck bridge in Middle Granville
31.7	Turn right onto Rt. 22A.
43.7	Center of Fair haven, Vt.
43.9	Follow Rt. 22A left around village green, stay on Rt. 22A.
44.8	Turn right to enter Rt. 4 east.
50.4	Park on shoulder of Rt. 4 by roadcut. It is legal to stop on this highway but vehicles must be pulled well off the road and should have flashers.

STOP 6

The purpose of this stop is to show the geometric and cross-cutting relations between the moderately east-dipping S_2 cleavage and the steeply east-dipping S_3 cleavage at the western edge of Domain B. Key features to observe include (1) the gradational change in the intensity of S_3 from a zone in which S_2 is dominant to a zone in which S_3 is dominant and (2) dissolution and folding of pre-existing layering and veins. Small lozenge-shaped blocks are commonly observed because of the angular relation between S_2 and S_3. In addition, asymmetrical folding of S_2 in which differentiation has resulted in coarser-grained hinges and finer-grained limbs can be observed.

	Proceed east on Rt. 4
50.7	Exit 5 from Rt. 4
50.9	Turn left onto Hubbarton Rd.
51.3	Park on right side of road.

STOP 7

The purpose of this stop is to show the main characteristics of the S_3 crenulation cleavage, where it is well developed in Domain B. Crenulation folds and evidence for pressure solution are well illustrated at this outcrop. Key features to observe include (1) differentiation associated with S_3 illustrated by coarse-grained fold hinges and fine-grained fold limbs, (2) the down-dip mineral lineation on the S_3 surface, defined mainly by chlorite and muscovite, and (3) dissolution and folding of pre-existing layering and veins. The spacing of the S_3 cleavage ranges from millimeters to centimeters.

	Turn around and retrace the route
51.6	Enter Rt. 4 east
57.1	Park well off the roadway.

STOP 8

The purpose of this stop is to show the geometric and cross-cutting relations between the S_3 and S_4 cleavages in Domain C. The S_4 cleavage is characterized by dissolution and newly developed phyllosilicate minerals in the cleavage domains. Key features to observe include (1) the relatively small spacing of the S_3 cleavage compared with that of the previous outcrop, (2) the spaced S_4 cleavage that crosscuts the steeply east-dipping S_3 cleavage, and (3) the lustrous S_4 surfaces and associated mineral lineation.

STOP 9 (Optional)

The purpose of this stop is to show the well developed S_4 cleavage. At this locality, the steeply dipping S_3 crenulation cleavage is almost completely overprinted. Key features to observe include (1) lustrous S_4 surfaces with a strong mineral lineation defined by phyllosilicates and (2) strongly folded and boudinaged pre-existing veins.